AJNR

Noninvasive Evaluation of Cerebral Arteriovenous Malformations by 4D-MRA for Preoperative Planning and Postoperative Follow-Up in 56 Patients: Comparison with DSA and Intraoperative Findings

D.R. Hadizadeh, G.M. Kukuk, D.T. Steck, J. Gieseke, H. Urbach, H.J. Tschampa, S. Greschus, A. Kovàcs, M. Möhlenbruch, A. Bostroem, H.H. Schild and W.A. Willinek

AJNR Am J Neuroradiol published online 2 February 2012
http://www.ajnr.org/content/early/2012/02/02/ajnr.A2921

Published February 2, 2012 as 10.3174/ajnr.A2921

Noninvasive Evaluation of Cerebral Arteriovenous Malformations by 4D-MRA for Preoperative Planning and Postoperative Follow-Up in 56 Patients: Comparison with DSA and Intraoperative Findings

ORIGINAL RESEARCH

D.R. Hadizadeh
G.M. Kukuk
D.T. Steck
J. Gieseke
H. Urbach
H.J. Tschampa
S. Greschus
A. Kovàcs
M. Möhlenbruch
A. Bostroem
H.H. Schild
W.A. Willinek

BACKGROUND AND PURPOSE: 4D-MRA is a promising technique in the diagnosis and follow-up of cAVMs. The purpose of this study was to compare 4D-MRA in the pre- and postoperative evaluation of cAVMs with DSA or intraoperative findings as the standards of reference regarding qualitative and quantitative parameters.

MATERIALS AND METHODS: Fifty-six consecutive patients with cAVMs (30 women) underwent both 4D-MRA and DSA. Preoperative 4D-MRA was excluded from analysis in 1 patient (movement artifacts). Twenty-five patients underwent surgery on cAVMs and underwent both imaging modalities pre- and postoperatively. 4D-MRA was performed with either 0.5-mol/L gadolinium-diethylene-triamine pentaacetic acid (group 1: voxel size, 1.1 × 1.1 × 1.4 mm^3; 608 ms/dynamic frame; 19 patients) or 1.0-mol/L gadobutrol (group 2: voxel size, 1.1 × 1.1 × 1.1 mm^3; 572 ms/dynamic frame; additional alternating view sharing; 37 patients). Two readers independently reviewed 4D-MRA and DSA regarding the Spetzler-Martin classification, arterial feeders, and postoperative residual filling. Vessel sharpness, vessel diameter, and VBC of 4D-MRA were quantified.

RESULTS: Preoperative Spetzler-Martin classification 4D-MRA and DSA ratings matched in 55/55 patients (Spetzler-Martin grades: I, 12; II, 22; III, 15; IV, 5; V, 1), and 93/100 arterial feeders were correctly identified by preoperative 4D-MRA (7 additional arterial feeders identified by DSA only: group 1, 3/19; group 2, 4/36). Postoperative 4D-MRA and DSA matched in 25/25 patients (residual filling, 1/25). Vessel sharpness and diameters did not differ substantially between the 2 groups. VBC was significantly higher in group 2 ($P < .005$).

CONCLUSIONS: 4D-MRA is a reliable tool that allows predicting Spetzler-Martin classification and postoperative residual filling; it hence allows substituting DSA in the pre- and postoperative evaluation of patients with cerebral AVMs.

ABBREVIATIONS: cAVM = cerebral arteriovenous malformation; CENTRA = contrast-enhanced timing-robust angiography; 4D-MRA = time-resolved MRA with subsecond temporal and high spatial resolution; FWHM = full width at half maximum, NSF = nephrogenic systemic fibrosis; VBC = vessel-to-background contrast

cAVMs are congenital focal abnormal conglomerations of dilated arteries and veins without a capillary bed and abnormal arteriovenous shunt surgery, having a prevalence of 0.01%–0.52% in the general population.[1] cAVMs are often diagnosed in young otherwise healthy patients and carry a lifelong bleeding risk of 2%–4% per year.[2] Treatment options include embolization, neurosurgical resection (in safely accessible lesions), and gamma knife radiosurgery or a combination of these techniques. Treatment is considered when the risk of hemorrhage outweighs risks associated with treatment. For postoperative/postinterventional follow-up and control examinations in nontreated cases, repetitive imaging studies are needed during a timeline of many years. The current standard of reference for visualization of cAVMs is DSA because it simultaneously provides high spatial and temporal resolution with clear visualization of feeding arteries and draining veins of these vascular abnormalities.[3-7] However, in addition to possible risks associated with repetitive radiation exposure and application of iodinated contrast agents including allergy and nephrotoxicity, limitations of DSA include risks of bleeding and stroke due to thromboembolism, with a risk for permanent neurologic deficits of 0.1%–1%.[8-11]

Therefore, noninvasive 4D-MRA with vastly accelerated acquisition techniques, which allow both high-temporal and high-spatial-resolution 3D visualization of the intracranial vasculature, may serve as an alternative noninvasive option for the diagnosis and follow-up of cAVMs.[5,12-14] However, the limitations of temporal and spatial resolution of 4D-MRA compared with DSA have been reported and primarily affect the identification of small feeding arteries.[15] The purpose of this study was to compare the performance of a highly advanced 4D-MRA protocol with DSA or intraoperative findings as standards of reference for the assessment of the pre- and postoperative evaluation of cAVMs.

Received July 15, 2011; accepted after revision August 17.

From the Departments of Radiology (D.R.H., G.M.K., D.T.S., J.G., H.U., H.J.T., S.G., A.K., M.M., H.H.S., W.A.W.) and Neurosurgery (A.B.), University of Bonn, Bonn, Germany; and Philips Healthcare (J.G.), Best, the Netherlands.

Please address correspondence to Dariusch R. Hadizadeh, MD, Department of Radiology, University of Bonn, Sigmund-Freud-Str. 25, D-53105 Bonn, Germany; e-mail: Dariusch.Hadizadeh@ukb.uni-bonn.de

http://dx.doi.org/10.3174/ajnr.A2921

Materials and Methods

Patients

Fifty-six (30 women, 26 men; average age, 39.0 ± 12.8 years; range, 18–69 years) consecutive patients with cAVMs were recruited between September 2004 and December 2010 (64 months) and underwent both 4D-MRA and DSA examinations. Before enrollment of patients into this study, the protocol was approved by the institutional ethics committee and written informed consent was obtained from all subjects. Patients older than 18 years who were scheduled for DSA because of suspected cAVMs were included in the study. Twenty-five of 56 patients underwent surgery for their cAVMs and underwent both imaging modalities pre- and postoperatively. In 1 case, preoperative 4D-MRA was nondiagnostic because the patient moved her head during contrast agent injection in the MR imaging unit. The same patient tolerated postoperative 4D-MRA well. In another case, postoperative DSA was waived because of the poor general condition of the patient due to postoperative vasospastic partial infarction of the right-sided middle cerebral artery territory. In this case, for data-analysis purposes, intraoperative findings instead of DSA served as the standard of reference regarding the presence of residual nidus filling.

4D-MRA

MR imaging studies were performed on 3T MR imaging whole-body scanners (Achieva 3.0 [19 patients, group 1] or 3.0 TX [37 patients, group 2]; maximum gradient amplitudes = 80 mT/m; slew rates= 200 T/m/s; Philips Healthcare, Best, the Netherlands) by using an 8-element head coil in all patients (the magnet was replaced during the 6-year recruitment period of the study). The following parameters were constant within all examinations: TR, 2.2 ms; TE, 0.9 ms; flip angle, 15°; FOV, 256 mm; parallel imaging (sensitivity encoding[16]) with an acceleration factor of 8 (phase encoding, 4; section encoding, 2); and half-Fourier imaging with 25% *k*-space reduction (acceleration factor = 1.33). Patients in group 1 (19/56) were examined with CENTRA keyhole[17-19] with a keyhole diameter of 16% (6-fold acceleration), and patients in group 2 (37/56) were examined by using CENTRA keyhole with a keyhole diameter of 20% and a view-sharing compression factor of 80 (total, 9-fold acceleration).[17-20]

Group 1 was imaged by using a matrix of 224 × 178, acquiring 50 dynamic datasets consisting of 140 sections each with a section thickness of 1.4 mm, resulting in a reconstructed voxel size of 1.1 × 1.1 × 1.4 mm^3. Group 2 was imaged by using a matrix of 232 × 232, acquiring 50 dynamic datasets consisting of 168 sections each with a section thickness of 1.1 mm, resulting in a reconstructed voxel size of 1.1 × 1.1 × 1.1 mm^3. In group 1, image update took place every 608 ms, whereas in group 2, the temporal resolution was 572 ms. While the image-update time was almost equal in both groups, there was a relevant change in spatial resolution leading to an acquired isotropic voxel size in the second group.

MR Imaging Contrast Agents

Two-phase injection protocols were used in all examinations. Group 1 (19 patients) received 20-mL 0.5-mol/L gadopentetate dimeglumine (Magnevist; Bayer Healthcare, Berlin, Germany), linear T1 relaxivity in blood (37°C/1.5T: 4.3 L $mmol^{-1}s^{-1}$) with flow rates of 3 mL/s (10 mL) and 1.5 (10 mL) mL/s. Group 2 (37 patients) received 10-mL 1.0-mol/L gadobutrol (Gadovist, Bayer Healthcare), macrocyclic T1 relaxivity in blood (37°C/1.5T: 5.3 L $mmol^{-1}s^{-1}$) with flow rates of 2 mL/s (5 mL) and 1 (5 mL) mL/s. Contrast agent application was followed by 30-mL saline flushes in all examinations. Data acquisition was started 10 seconds after first injection of contrast media in all examinations.

Conventional Angiography

DSA was performed on a biplane Integris V 5000 (Philips Healthcare) with a 5F catheter that was navigated into the internal carotid, external carotid, and both vertebral arteries via the transfemoral route in 56/56 patients. The images were acquired after manual injection of 5–7 mL of iopromide (Ultravist; Bayer Healthcare). Frame rates were 3/s in the arterial phase, 2/s in the venous phase, and 8 frames/s in the fast angiographic series.

Qualitative Analysis

Datasets were independently reviewed by 3 readers (2 readers of 4D-MRA, 1 reader of DSA). Data analysis included the Spetzler-Martin classification[21] (covering nidus size: I = 0–3 cm, II = 3–6 cm, III = >6 cm; the venous drainage pattern: 0 = superficial, I = deep, and eloquence of adjacent brain: 0/I), the identification of feeding arteries, and postoperative assessment of complete resection of the lesion-versus-residual filling of the nidus. Readings of DSA images and 4D-MRA datasets by using originally acquired sections, multiplanar reformats, and maximum intensity projections were performed independently by the 3 readers (1 DSA, 2 4D-MRA) on a standard postprocessing workstation.

Quantitative Analysis

Estimates of the vessel contrast, vessel sharpness, and vessel width were calculated by using line profile plots perpendicular to the vessel track.[22] Measurements were performed in large, medium-sized, and small intracranial arteries and veins, respectively, including the internal cerebral artery (A1), the middle cerebral artery (A2), and the proximal A3-segment of the anterior cerebral artery (A3) as well as the superior sagittal sinus (V1), the straight sinus (V2), and the inferior sagittal sinus (V3). To guarantee analysis at corresponding enhancement levels, we standardized dynamic time frames for quantitative measurements (3 seconds after initial arterial bolus arrival for all arterial vessels and 3 seconds after the initial venous bolus arrival for all venous vessels). Line profile plots were created with a public domain image-processing software (ImageJ, National Institutes of Health, Bethesda, Maryland).

VBC was measured as the quotient of the difference of vessel signal-intensity level to background signal-intensity level and the sum of vessel-signal intensity level to background signal-intensity level as described earlier.[23] This approach was chosen instead of contrast-to-noise measurements to avoid noise quantification, which has been shown to be inconsistent when parallel imaging techniques are applied.[24] The reciprocal of the sum of distances between 25% and 75% of maximum intensity was selected as an indicator for the steepness of the line-enhancement profile to estimate vessel sharpness as shown in Fig 1*A*.[22] The FWHM of the line-enhancement profile served as an estimate of the vessel width (Fig 1*B*).[25]

Statistics

The Kendall coefficient of concordance was computed to compare the 2 readers in their assessment of image quality, level of confidence, and Spetzler-Martin classification by using 4D-MRA and to compare intermodality agreement of the Spetzler-Martin classification as determined by DSA and 4D-MRA. Kendall coefficients of 0.5–0.8 were considered to indicate good agreement, and coefficients higher than

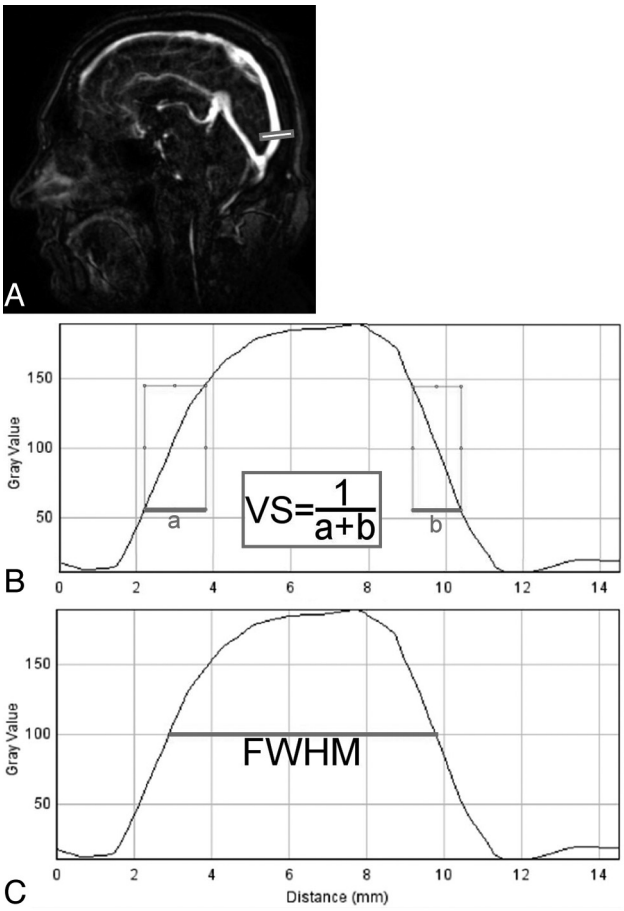

Fig 1. Quantitative measurements for assessment of vessel sharpness and estimated vessel width of 4D-MRA of intracranial vessels. *A*, Sagittal original section of the 4D MRA dataset and the site of measurement in the superior sagittal sinus (*bar*). *B* and *C*, Line-enhancement profile curves were used to estimate vessel sharpness by the reciprocal of the sum of the distances from 25% to 75% maximum-enhancement levels (*thick lines*, formula in the middle bar, *B*) and vessel width as the FWHM of the given profile (*C*).

0.8 were considered to indicate excellent agreement. Estimates of vessel contrast, vessel sharpness, and vessel width in groups 1 and 2 were compared by using the Student *t* test. All statistical analyses were performed with the Statistical Package for the Social Sciences, Version 11.0 (SPSS, Chicago, Illinois).

Only those authors who were not employees of Philips Healthcare had control of inclusion of any data and information that might present a conflict (author J.G.) is an employee of this company). Before this study, Philips Healthcare provided technical assistance for sequence optimization.

Results

4D-MRA was successfully performed in 80/81 (98.8%) examinations (56 preoperative examinations, 25 postoperative examinations). In 1 patient (group 2), preoperative 4D-MRA was nondiagnostic due to movement of the patient during data acquisition. This examination was excluded from quantitative and qualitative data analysis regarding the Spetzler-Martin classification and identification of arterial feeders, leaving 55 preoperative and 25 postoperative examinations for data analysis. In the same patient, postoperative 4D-MRA was successfully performed without movement artifacts. No adverse events from either of the applied contrast agents were observed.

Qualitative Analysis

The preoperative Spetzler-Martin classification by 4D-MRA and DSA matched in 55/55 patients ($\kappa = 1$). Spetzler-Martin grades were rated as follows: grade I, 12/55 (21.8%) patients; grade II, 22/55 (40%) patients; grade III, 15/55 (27.3%) patients; grade IV, 5/55 (9.1%) patients; and grade V, 1/55 (1.8%) patients.

Ninety-three of 100 (93%) feeding arteries (group 1: 36/39; 92.3%; group 2: 57/61, 93.4%) were identified by 4D-MRA and confirmed by DSA in 55 patients with preoperative 4D-MRA and DSA. Additional arterial feeders were identified by DSA only in 7 patients, including 3/19 patients (15.8%) in group 1 and 4/36 patients (11.1%) in group 2. There was no change in operative management in any case.

Surgical resection was performed in 25/56 (44.6%) patients (Fig 2). Readings of postoperative 4D-MRA and DSA confirmed complete resection of the nidus in 24/25 (96%) patients. Interobserver and intermodality agreement was excellent in all cases ($\kappa = 1$). In 1/25 patients, 4D-MRA revealed residual nidus filling; the residual filling was confirmed by intraoperative evaluation as the standard of reference in this case (Fig 3).

Quantitative Analysis

Estimates of the vessel sharpness and vessel width revealed no substantial differences for the 2 groups that were scanned with different protocols and contrast agents. While the vessel sharpness was estimated at 9.2% higher in the lacerum segment of the internal cerebral artery in the second group, this parameter was estimated at 20.6% lower in the inferior sagittal sinus in the same group; all other vessels showed no significant differences in vessel-sharpness estimates (Table 1). The estimated vessel width, defined as the full width of the line profile at half maximum intensity, was measured at 17.8% higher in the second group in the inferior sagittal sinus, whereas all other measurements revealed no significant differences (Table 2).

Significantly higher VBC was quantified in group 2 for all vessel segments ($P < .01$). In general, contrast measurements revealed higher values for larger arterial and venous vessels. VBC was increased in the second group in large vessels (4.9% and 7.4% in the lacerum segment of the internal cerebral artery and the superior sagittal sinus, respectively). In medium-sized vessels, the increase in VBC was more pronounced (11.5% and 11.1% in the M1 segment of the middle cerebral artery and the straight sinus, respectively). The largest increase of VBC was observed in the small vessels with an increase of 18.5% in the A3 segment of the anterior cerebral artery and an increase of 67.8% in the inferior sagittal sinus. Increases in VBC were consistently observed for vessels in all patients.

Discussion

Detailed information on the angioarchitecture and flow dynamics of cAVMs obtained by noninvasive imaging techniques is essential as an alternative to DSA in the diagnosis and follow-up of these lesions, even though it may not fully substitute for DSA at the current stage.[26] Image-update rates in DSA in our study ranged from 2 to 8 frames per second. At the expense of a higher patient dose, even higher frame rates are possible with modern conventional angiography units. At the

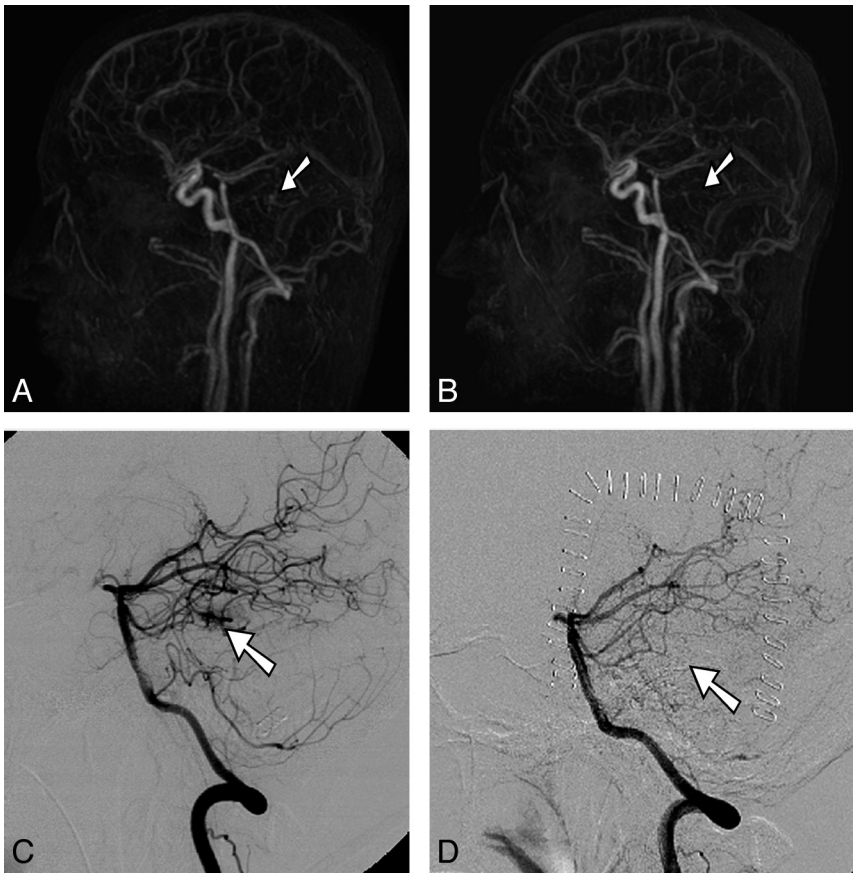

Fig 2. Pre- and postoperative 4D-MRA and DSA in a 21-year-old man with a small left temporal cAVM, grade II (Spetzler-Martin classification). *A* and *C*, In preoperative full-volume lateral maximum-intensity-projection 4D-MRA (*A*) and selective DSA via the left vertebral artery (*C*), the small nidus is visualized. *B* and *D*, In postoperative full-volume lateral maximum-intensity-projection 4D-MRA (*B*) and selective DSA via the left vertebral artery (*D*), complete resection of the lesion is verified.

same time, the in-plane spatial resolution by using a 1024 × 1024 matrix, depending on the selected image intensifier size (170–380 mm), ranged from 0.17 × 0.17 to 0.37 × 0.37 mm^2. Compared with these numbers, 4D-MRA with an image-update time of 2 frames/s at an in-plane spatial resolution of 1.1 × 1.1 mm^2 is far behind the possibilities of spatial and temporal resolution in DSA. However, the noninvasiveness of 4D-MRA allows repeated low-risk examinations, especially of patients with treated cAVMs. Furthermore, the availability of dynamic 3D datasets may partly compensate for the nonselectivity of contrast agent application to a specific vessel in 4D-MRA. We present intraindividual comparisons of 4D-MRA and DSA that were collected over a recruitment period of >6 years in 56 patients with cAVMs. The study population included 25 patients who underwent surgery for their malformations and who received both pre- and postoperative imaging or intraoperative comparison.

Qualitative Analysis

The qualitative analysis of our data reinforces earlier results concerning the reliability of preoperative Spetzler-Martin classification of cAVMs by using noninvasive 4D-MRA, including 2 subgroups that received 4D-MRA either with or without the implementation of view-sharing and with either 0.5-mol/L gadopentetate dimeglumine or 1.0-mol/L gadobutrol.[15] The identification of small feeding arteries remains challenging by using 4D-MRA. However, in the subgroup that was examined with the later generation MR imaging scanner with implementation of alternating view sharing (with increased spatial and temporal resolution) and the high-molarity contrast agent, 1.0-mol/L gadobutrol, feeding arteries were missed by 4D-MRA in fewer patients. To overcome the limitation concerning the identification of these small vessels, Saleh et al[27] proposed acquiring both a high-temporal-resolution 4D-MRA and a static high-spatial-resolution 3D-MRA. This approach may further benefit from the implementation of a very high-spatial-resolution time-of-flight technique with a 1024+ matrix.[28]

Quantitative Analysis

FWHM measurements revealed no significant differences in the estimated diameter of small, medium-sized, and large intracranial arteries and veins except a significantly increased diameter of the inferior sagittal sinus in the second group. The measurement of larger vessel diameters may be due to blurring that apparently mainly affects small intracranial veins, and this might be caused by a relative increase in undersampling in view sharing in relation to the reference image. However, differences between the 2 groups concerning the sharpness and estimated vessel width of the V3 segment (Tables 2 and 3) had no impact on the classification of venous drainage patterns of cAVMs in our study population. A general tendency for over- and underestimation of vessel size from 1 group to the other was not observed, and the otherwise consistent vessel-width

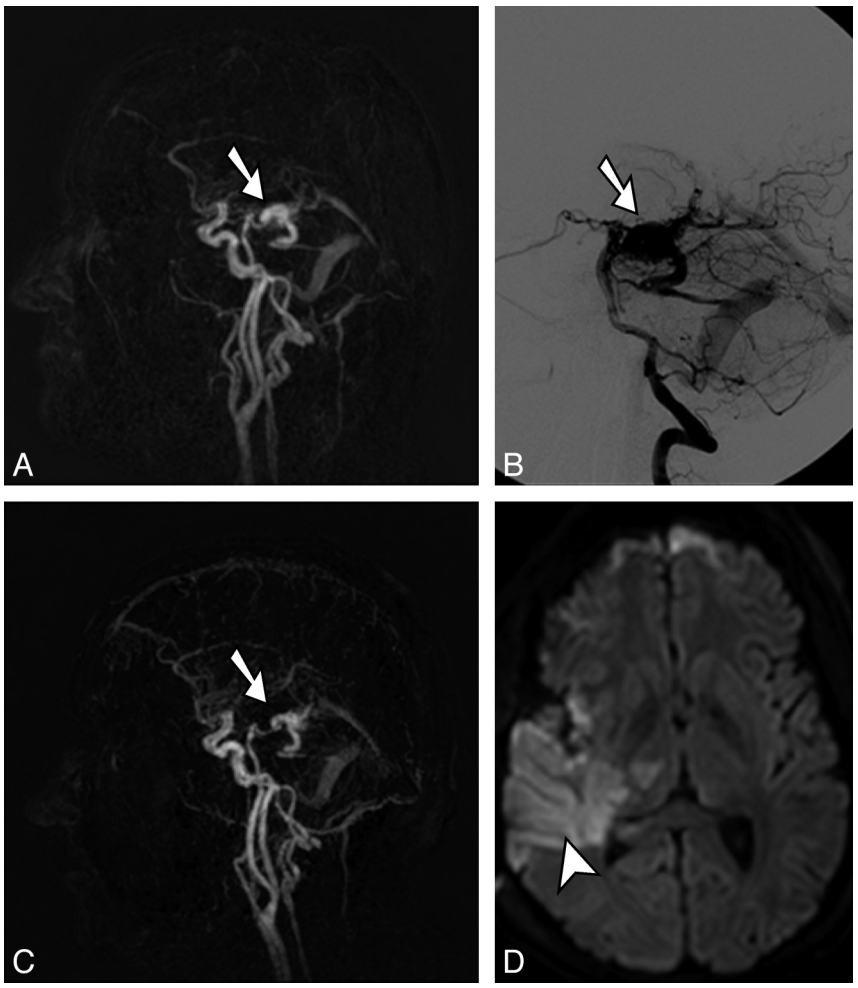

Fig 3. Pre- and postoperative 4D-MRA and postoperative transversal diffusion-weighted image ($b = 1000$) in a 23-year-old man with a right temporal cAVM grade II (Spetzler-Martin classification). The nidus (*arrows*) is visualized accordingly in preoperative full-volume lateral maximum-intensity-projection 4D-MRA (*A*) and selective DSA via the right vertebral artery (*B*). Only a few small arterial feeders could be occluded intraoperatively, and resection of the nidus was not possible. *C*, Postoperative full-volume lateral maximum-intensity-projection 4D-MRA reveals residual filling of the nidus (*arrow*) according to the operative site, and a transversal diffusion-weighted image confirms a partial infarction of the right middle cerebral artery territory (*arrowhead*) and parts of the right thalamus.

Table 1: Estimates of vessel sharpness (1 mm) defined as the reciprocal sum of the width from 25% to 75% of the maximum intensity increase in 3 arterial and 3 venous vessel segments and decreasing vessel diameters

	All	Group 1	Group 2	*T* Test
A1	0.39 ± 0.04	0.37 ± 0.03	0.40 ± 0.04	.0010[a]
A2	0.41 ± 0.08	0.41 ± 0.10	0.41 ± 0.07	.4896
A3	0.47 ± 0.10	0.47 ± 0.12	0.47 ± 0.09	.4928
V1	0.30 ± 0.05	0.28 ± 0.04	0.30 ± 0.05	.0648
V2	0.35 ± 0.06	0.37 ± 0.08	0.34 ± 0.06	.0543
V3	0.52 ± 0.15	0.62 ± 0.24	0.49 ± 0.11	.0016[a]

Note:—A1 indicates internal cerebral artery (lacerum segment, large artery); A2, middle cerebral artery (proximal segment "M1," medium-sized artery); A3, anterior cerebral artery (small artery); V1, superior sagittal sinus (1 cm proximal of the confluens, large vein); V2, straight sinus (1 cm proximal of the confluens, medium-sized vein); V3, inferior sagittal sinus (1 cm proximal to the straight sinus, small vein).
[a] Significant ($P < .05$).

Table 2: Estimated vessel width FWHM (millimeters) defined as the full width of the line profile at 50% of the maximum intensity increase in 3 arterial and 3 venous vessel segments and decreasing vessel diameters

	All	Group 1	Group 2	*T* Test
A1	4.22 ± 0.58	4.23 ± 0.72	4.22 ± 0.55	.4812
A2	3.28 ± 0.47	3.31 ± 0.53	3.28 ± 0.45	.4105
A3	2.84 ± 0.45	2.88 ± 0.37	2.83 ± 0.47	.3345
V1	6.52 ± 1.31	6.67 ± 1.87	6.48 ± 1.14	.3135
V2	4.20 ± 0.69	4.02 ± 0.86	4.25 ± 0.64	.1269
V3	2.57 ± 0.55	2.25 ± 0.56	2.65 ± 0.52	.0055[a]

[a] Significant ($P < .05$).

estimates may serve as a measure for reproducibility of the acquired data independent of the change in MR imaging scanners, imaging protocols, and contrast agents during the recruitment period.

The second measured quantitative parameter, estimated vessel sharpness, was not significantly different within the study groups for most vessels; this finding indicated that the implementation of view sharing in the second group did not generally cause significant blurring effects, which may be a concern when temporal interpolation techniques are applied. The significant and consistent increase in vessel-to-background contrast in the second group, on the other hand, may be best explained by the change from a standard (0.5 mol/L) to a high-molarity (1.0 mol/L) contrast agent. Similarly, a better contrast of small arteries with a 1.0-mol/L contrast agent compared with a 0.5-mol/L contrast agent was observed in abdominal vessels at an equimolar dosage.[23]

Table 3: Vessel-to-background measurements in 3 arterial and 3 venous vessel segments and decreasing vessel diameters

	All	Group 1	Group 2	*T* Test
A1	0.92 ± 0.05	0.88 ± 0.07	0.93 ± 0.04	.0008[a]
A2	0.84 ± 0.11	0.77 ± 0.15	0.85 ± 0.10	.0035[a]
A3	0.65 ± 0.13	0.56 ± 0.12	0.67 ± 0.13	.0034[a]
V1	0.91 ± 0.05	0.86 ± 0.05	0.92 ± 0.04	.0000[a]
V2	0.83 ± 0.10	0.76 ± 0.15	0.85 ± 0.08	.0018[a]
V3	0.52 ± 0.19	0.34 ± 0.23	0.56 ± 0.15	.0000[a]

[a] Significant ($P < .05$).

Posttreatment Follow-Up

Using static contrast-enhanced time-of-flight MR angiography at 3T in 32 patients with radiosurgical treatment of cAVMs, Lee et al[29] found that the sensitivity of their method was high but the specificity was not sufficient for the detection of residual AVMs after radiosurgery. With our time-resolved high-spatial-resolution protocol, noninvasive 4D-MRA was able to correctly judge whether there was residual filling of the nidus after surgical resection with 100% agreement compared with DSA; in the case in which the surgical nidus resection was not successful, 4D-MRA was able to correctly demonstrate residual nidus filling according to the operative situs. The fact that 4D-MRA can be implemented within a regular MR imaging protocol together with structural MR imaging allowed simultaneous visualization of a partial infarction of the right middle cerebral artery territory, providing important information for postoperative management. At the same time, invasive DSA in this patient was waived because of the poor general condition of the patient at that time, and 4D-MRA was the only technique to dynamically document residual nidus filling, which was confirmed by surgery. While 4D-MRA may not fully substitute for DSA, given the current spatial and temporal resolution, it proved to be a valuable alternative to DSA, which may, for instance, be of value in selected cases (eg, in the patient with a residual cAVM in our study) in which DSA is not available.

Outlook

4D-MRA is also increasingly recognized as a diagnostic tool for spinal and cranial arteriovenous fistulas, in which the visualization of angioarchitecture and flow dynamics is crucial for possible partial replacement of DSA.[30-32] Further studies will be needed to evaluate the role of 4D-MRA in arteriovenous malformations in all body regions. Other techniques have been developed for time-resolved MRA of intracranial vessels including undersampling *k*-space techniques such as time-resolved imaging of contrast kinetics (TRICKS),[33] time-resolved echo-shared angiography technique (TREAT),[12,34] phase contrast highly constrained back-projection reconstruction (PC-HYPR),[35] flow-sensitive 4D-MRA,[36] and, more recently, unenhanced dynamic MRA by using true free induction with steady-state precession–based spin-tagging with alternating radio-frequency.[37] Promising first results have been presented by using these techniques, which will require further evaluation in clinical trials with the ultimate goal of substituting them for DSA in the future.[38,39]

The change of equipment and contrast agents during the recruitment period of this study allows evaluation of the impact of 2 different scan protocols and the application of a high-molar macrocyclic contrast agent instead of a standard-molarity linear contrast agent. Qualitative and quantitative parameters show that the combination of the CENTRA keyhole technique with alternating view sharing does not lead to substantial additional artifacts and allows an increase of spatial resolution to an isotropic 1.1-mm voxel with no penalty in temporal resolution. The change in contrast agents resulted in a higher VBC of both arteries and veins. In addition to the observed higher contrast of the higher molarity contrast agent, the change from a linear to a macrocyclic contrast agent may be beneficial because of different profiles concerning the risk for NSF: The European Medicines Agency (EMEA) lists 1.0-mol/L gadobutrol as a low-risk agent for the development of NSF, whereas the standard-molarity linear contrast agent that was used before the FDA announced its warning on NSF for gadolinium-containing contrast agents has been classified as a high-risk agent by the same institution (EMEA).[40] Otherwise, differences in toxicity of the 2 contrast agents have not been reported, to our knowledge. Furthermore, additional studies will be necessary to further elucidate the added impact of injection rates on image quality.[41]

Conclusions

High-spatial- and high-temporal-resolution 4D-MRA compared with DSA allows accurate preoperative Spetzler-Martin classification of cAVMs and reliable postoperative assessment of residual nidus filling. Additional view sharing with isotropic spatial resolution and the application of 1.0-mol/L gadobutrol allows a significantly higher vessel-to-background contrast and the identification of feeding arteries in more patients. 4D-MRA is a reliable tool for preoperative characterization of cAVMs and a valuable addition to postoperative follow-up after surgical removal of the lesion. This may allow a reduction of invasive and sometimes repetitive follow-up DSA examinations in this predominantly young population, even though it may not fully replace DSA at the current stage due to limitations in spatial and temporal resolution

Disclosures: Guido Kukuk—*UNRELATED: Payment for Lectures (including service on Speakers Bureaus)*: Bayer Healthcare, Philips Healthcare. Jürgen Gieseke—*UNRELATED: Employment*: Philips Healthcare, *Comments*: only research in the university. Winfried A. Willinek—*UNRELATED: Payment for Lectures (including service on Speakers Bureaus)*: GE Healthcare, Bracco, Philips Healthcare, Bayer Healthcare, Lantheus Medical Imaging, *Payment for Development of Educational Presentations*: GE Healthcare, Bracco, Philips Healthcare, Bayer Healthcare, Lantheus Medical Imaging.

References

1. Friedlander RM. **Clinical practice: arteriovenous malformations of the brain.** *N Engl J Med* 2007;356:2704–12
2. Kondziolka D, McLaughlin MR, Kestle JR. **Simple risk predictions for arteriovenous malformation hemorrhage.** *Neurosurgery* 1995;37:851–55
3. Du J, Fain SB, Korosec FR, et al. **Time-resolved contrast-enhanced carotid imaging using undersampled projection reconstruction acquisition.** *J Magn Reson Imaging* 2007;25:1093–99
4. Mistretta CA, Grist TM, Korosec FR, et al. **3D time-resolved contrast-enhanced MR DSA: advantages and tradeoffs.** *Magn Reson Med* 1998;40:571–81
5. Willinek WA, Hadizadeh DR, von Falkenhausen M, et al. **4D time-resolved MR angiography with keyhole (4D-TRAK): more than 60 times accelerated MRA using a combination of CENTRA, keyhole, and SENSE at 3.0T.** *J Magn Reson Imaging* 2008;27:1455–60
6. Eddleman CS, Jeong HJ, Hurley MC, et al. **4D radial acquisition contrast-enhanced MR angiography and intracranial arteriovenous malformations: quickly approaching digital subtraction angiography.** *Stroke* 2009;40:2749–53
7. Warren DJ, Hoggard N, Walton L, et al. **Cerebral arteriovenous malformations: comparison of novel magnetic resonance angiographic techniques and conventional catheter angiography.** *Neurosurgery* 2007;61:187–96

8. Dion JE, Gates PC, Fox AJ, et al. **Clinical events following neuroangiography: a prospective study.** *Stroke* 1987;18:997–1004
9. Earnest F, Forbes G, Sandok BA, et al. **Complications of cerebral angiography: prospective assessment of risk.** *AJR Am J Roentgenol* 1984;142:247–53
10. Johnston DC, Chapman KM, Goldstein LB. **Low rate of complications of cerebral angiography in routine clinical practice.** *Neurology* 2001;57:2012–14
11. Willinsky RA, Taylor SM, TerBrugge K, et al. **Neurologic complications of cerebral angiography: prospective analysis of 2,899 procedures and review of the literature.** *Radiology* 2003;227:522–28
12. Gauvrit JY, Law M, Xu J, et al. **Time-resolved MR angiography: optimal parallel imaging method.** *AJNR Am J Neuroradiol* 2007;28:835–38
13. Reinacher P, Reinges MH, Simon VA, et al. **Dynamic 3-D contrast-enhanced angiography of cerebral tumours and vascular malformations.** *Eur Radiol* 2007;17(suppl 6):F52–62
14. Petkova M, Gauvrit JY, Trystram D, et al. **Three-dimensional dynamic time-resolved contrast-enhanced MRA using parallel imaging and a variable rate k-space sampling strategy in intracranial arteriovenous malformations.** *J Magn Reson Imaging* 2009;29:7–12
15. Hadizadeh DR, von Falkenhausen M, Gieseke J, et al. **Cerebral arteriovenous malformation: Spetzler-Martin classification at subsecond-temporal-resolution four-dimensional MR angiography compared with that at DSA.** *Radiology* 2008;246:205–13
16. Pruessmann KP, Weiger M, Scheidegger MB, et al. **SENSE: sensitivity encoding for fast MRI.** *Magn Reson Med* 1999;42:952–62
17. Jones RA, Haraldseth O, Muller TB, et al. **K-space substitution: a novel dynamic imaging technique.** *Magn Reson Med* 1993;29:830–34
18. van Vaals JJ, Brummer ME, Dixon WT, et al. **"Keyhole" method for accelerating imaging of contrast agent uptake.** *J Magn Reson Imaging* 1993;3:671–75
19. Willinek WA, Gieseke J, Conrad R, et al. **Randomly segmented central k-space ordering in high-spatial-resolution contrast-enhanced MR angiography of the supraaortic arteries: initial experience.** *Radiology* 2002;225:583–88
20. Hadizadeh DR, Gieseke J, Beck G, et al. **View-sharing in keyhole imaging: partially compressed central k-space acquisition in time-resolved MRA at 3.0T.** *Eur J Radiol* 2011;80:400–06. Epub 2010 May 5
21. Spetzler RF, Martin NA. **A proposed grading system for arteriovenous malformations.** *J Neurosurg* 1986;65:476–83
22. Naehle CP, Kaestner M, Muller A, et al. **First-pass and steady-state MR angiography of thoracic vasculature in children and adolescents.** *JACC Cardiovasc Imaging* 2010;3:504–13
23. Hadizadeh DR, von Falkenhausen M, Kukuk GM, et al. **Contrast material for abdominal dynamic contrast-enhanced 3D MR angiography with parallel imaging: intraindividual equimolar comparison of a macrocyclic 1.0 M gadolinium chelate and a linear ionic 0.5 M gadolinium chelate.** *AJR Am J Roentgenol* 2010;194:821–29
24. Buerke B, Allkemper T, Kugel H, et al. **Qualitative and quantitative analysis of routinely postprocessed (CLEAR) CE-MRA data sets: are SNR and CNR calculations reliable?** *Acad Radiol* 2008;15:1111–17
25. Etienne A, Botnar RM, Van Muiswinkel AM, et al. **"Soap-Bubble" visualization and quantitative analysis of 3D coronary magnetic resonance angiograms.** *Magn Reson Med* 2002;48:658–66
26. Geibprasert S, Pongpech S, Jiarakongmun P, et al. **Radiologic assessment of brain arteriovenous malformations: what clinicians need to know.** *Radiographics* 2010;30:483–501
27. Saleh RS, Lohan DG, Villablanca JP, et al. **Assessment of craniospinal arteriovenous malformations at 3T with highly temporally and highly spatially resolved contrast-enhanced MR angiography.** *AJNR Am J Neuroradiol* 2008;29:1024–31
28. Willinek WA, Gieseke J, von Falkenhausen M, et al. **Sensitivity encoding (SENSE) for high spatial resolution time-of-flight MR angiography of the intracranial arteries at 3.0 T.** *Rofo* 2004;176:21–26
29. Lee KE, Choi CG, Choi JW, et al. **Detection of residual brain arteriovenous malformations after radiosurgery: diagnostic accuracy of contrast-enhanced three-dimensional time of flight MR angiography at 3.0 Tesla.** *Korean J Radiol* 2009;10:333–39
30. Nishimura S, Hirai T, Sasao A, et al. **Evaluation of dural arteriovenous fistulas with 4D contrast-enhanced MR angiography at 3T.** *AJNR Am J Neuroradiol* 2010;31:80–85
31. Farb RI, Agid R, Willinsky RA, et al. **Cranial dural arteriovenous fistula: diagnosis and classification with time-resolved MR angiography at 3T.** *AJNR Am J Neuroradiol* 2009;30:1546–51
32. Ali S, Cashen TA, Carroll TJ, et al. **Time-resolved spinal MR angiography: initial clinical experience in the evaluation of spinal arteriovenous shunts.** *AJNR Am J Neuroradiol* 2007;28:1806–10
33. Wu Y, Kim N, Korosec FR, et al. **3D time-resolved contrast-enhanced cerebrovascular MR angiography with subsecond frame update times using radial k-space trajectories and highly constrained projection reconstruction.** *AJNR Am J Neuroradiol* 2007;28:2001–04
34. Fink C, Ley S, Kroeker R, et al. **Time-resolved contrast-enhanced three-dimensional magnetic resonance angiography of the chest: combination of parallel imaging with view sharing (TREAT).** *Invest Radiol* 2005;40:40–48
35. Velikina JV, Johnson KM, Wu Y, et al. **PC HYPR flow: a technique for rapid imaging of contrast dynamics.** *J Magn Reson Imaging* 2010;31:447–56
36. Wetzel S, Meckel S, Frydrychowicz A, et al. **In vivo assessment and visualization of intracranial arterial hemodynamics with flow-sensitized 4D MR imaging at 3T.** *AJNR Am J Neuroradiol* 2007;28:433–38
37. Yan L, Wang S, Zhuo Y, et al. **Unenhanced dynamic MR angiography: high spatial and temporal resolution by using true FISP-based spin tagging with alternating radiofrequency.** *Radiology* 2010;256:270–79
38. Fatima Z, Ishigame K, Hori M, et al. **Time-resolved contrast-enhanced magnetic resonance digital subtraction angiography (MRDSA) in an infant with congenital pial arteriovenous fistula in the brain: a case report.** *Childs Nerv Syst* 2010;26:1121–24
39. Cashen TA, Carr JC, Shin W, et al. **Intracranial time-resolved contrast-enhanced MR angiography at 3T.** *AJNR Am J Neuroradiol* 2006;27:822–29
40. European Medicines Agency. **European Medicines Agency makes recommendations to minimise risk of nephrogenic systemic fibrosis with gadolinium-containing contrast agents.** http://www.ema.europa.eu/docs/en_GB/document_library/Referrals_document/gadolinium_31/WC500015635.pdf. Accessed November 15, 2011.
41. Kramer H, Michaely HJ, Requardt M, et al. **Effects of injection rate and dose on image quality in time-resolved magnetic resonance angiography (MRA) by using 1.0M contrast agents.** *Eur Radiol* 2007;17:1394–402. Epub 2006 Nov 18